Acoustics Australia (2020) 48:407–418
https://doi.org/10.1007/s40857-020-00194-2

ORIGINAL PAPER

Efficient Acoustic Topology Optimization Using Vibro-Acoustic Coupled Craig–Bampton Mode Synthesis

Xudong Wang[1] · **Deshi Wang**[1] · **Bao Liu**[2]

Received: 18 March 2020 / Accepted: 1 July 2020 / Published online: 17 July 2020

Abstract
Continuum topology optimization is an effective way to reduce vibration and noise of vibro-acoustic coupling system. However, the high computation time required for calculating the vibro-acoustic responses during topology optimization is a major obstacle for practical applications. In this paper, a novel symmetric method of vibro-acoustic system matrix is proposed, and a new model reduction method is developed based on Craig–Bampton mode synthesis method to compute dynamic responses with adequate efficiency and accuracy for topology optimization. The comparison results show that the proposed method substantially reduces the degrees of freedom (DOFs) and calculation time. The response values and eigenfrequencies calculated by the model reduction method are exactly the same as those of the full model. Furthermore, the bidirectional evolutionary structural optimization (BESO) algorithm is applied to solve the problem of minimizing the response of a single frequency and a certain range of frequency excitation at a specified target point. The results show that the optimization algorithm converges fast, the iterative process is robust and the response values of different coupling systems can be reduced to a higher extend, which indicates the applicability of the optimization algorithm.

Keywords Model reduction · Vibro-acoustic interaction · Topology optimization · Multiobjective optimization · Frequency response · BESO

1 Introduction

Continuum topology optimization is a practical method for reducing vibration and noise of structures by changing the distribution of structural materials [1]. Scholars have achieved certain results in this regard [2–5]. However, topology optimization requires multiple iterations to obtain the optimal solution until convergence. For large-scale complex systems, the ever-increasingly complex phenomena of finite element models with numbers of DOFs and the iterative optimizing process will generate a huge amount of calculations. Therefore, it is necessary to study the processing methods for large-scale optimization systems.

✉ Xudong Wang
wanghsutung@163.com

[1] College of Weaponry Engineering, Naval University of Engineering, Wuhan 430033, Hubei, People's Republic of China

[2] College of Electronic Engineering, Naval University of Engineering, Wuhan 430033, Hubei, People's Republic of China

To reduce the calculation time in the optimization process, many scholars have taken efforts to do this. For the problem of high computational complexity of element sensitivity in the optimization process, Chu [6] proposed that the adjoint method can effectively reduce the complexity of sensitivity analysis of frequency response problems. But this method still has a large amount of calculation on multifrequency problems. Jensen [7] proposed a method based on the PADE approximation method and the analytical sensitivity derived from the adjoint method with low calculation costs for the sensitivity of multiple design variables in a wide frequency range. Allaire [8] calculated the standard adjoint vector based on the classic modal method. An adjoint variable method for the response sensitivity analysis was proposed by Kang [9] in investigating the optimal distribution of damping material subject to harmonic excitations. Numerical examples were presented for confirming the efficiency and correctness of this approach.

Another approach is to transform complex dynamic problems into static problems. Choi [10] employed the principle of equivalent static load (ESL) to propose a quasi-static optimization method for structures under dynamic loading,

which enables us to optimize structures with dynamic loads. Zhao [11] and Lee [12] conducted further research with the objective of minimizing structural flexibility and dynamic response, and established a topology optimization method for structural dynamic stiffness based on the equivalent static loads method. To realize the topology optimization design under the dynamic multiobjective structure, a progressive structural topology optimization model is proposed. The model takes the weighting function that maximizes the natural frequency and minimizes the dynamic flexibility of a specific mode as the objective function [13]. Reducing the size of the system matrix before calculating the structural response using the model reduction method is more efficient than the above methods. Due to the advantages of high calculation accuracy, Craig–Bampton method [14] has received extensive attention. Many innovative model reduction methods based on Craig–Bampton method have been developed [15, 16], and this method is extended to the vibro-acoustic coupling problems [17–19]. However, its application to vibro-acoustic topology optimization has not been studied or developed before this research. The existing methods are only for the optimization of dynamic and static characteristics of some simple structural systems.

To contribute to the research subject of vibro-acoustic response, this study proposes a novel vibro-acoustic coupling matrix symmetry method, which realizes the application of the Craig–Bampton modal synthesis method to the vibro-acoustic coupling response solution without affecting the accuracy of calculation results. After that, its applications for efficient topology optimization have been proposed to reduce the noise level of the target point as the objective function.

This paper is organized as follows. A new symmetric vibro-acoustic formulation and model reduction of structure-acoustic coupling system based on Craig–Bampton method are introduced in Sect. 2. In Sect. 3, sensitivity analysis and topology optimization algorithm are presented. Then, in Sect. 4, numerical examples are presented to demonstrate the efficiency and accuracy of the proposed method. Section 5, we conclude the paper.

2 Structure-Acoustic Coupled Mode Synthesis Method

2.1 Structure-Acoustic Coupling Equations

The structure-acoustic coupling system with finite displacement is based on the assumption of ideal fluid with little viscosity and compressibility, and linear elasticity structure with small deformations. The coupling conditions at the boundary between the structural and acoustic domains ensure the continuity in displacement and pressure between the domains.

Taking the structural displacement u_s and the fluid displacement potential ψ_f as the basic variables [20], the Galerkin method with weighted margins is used to obtain the finite element equation of vibro-acoustic coupling system:

$$\begin{bmatrix} \boldsymbol{M}_s & \rho \boldsymbol{H} \\ \boldsymbol{0} & \boldsymbol{M}_f \end{bmatrix} \begin{bmatrix} \ddot{\boldsymbol{u}}_s \\ \ddot{\boldsymbol{\psi}}_f \end{bmatrix} + \begin{bmatrix} \boldsymbol{K}_s & \boldsymbol{0} \\ -c^2 \boldsymbol{H}^T & \boldsymbol{K}_f \end{bmatrix} \begin{bmatrix} \boldsymbol{u}_s \\ \boldsymbol{\psi}_f \end{bmatrix} = \begin{bmatrix} \boldsymbol{f}_s \\ \boldsymbol{0} \end{bmatrix} \tag{1}$$

where $\boldsymbol{K}_s$ and $\boldsymbol{K}_f$ are the system stiffness matrix of the structure domain and the acoustic domain, $\boldsymbol{M}_s$ and $\boldsymbol{M}_f$ are the system mass matrix of the structure domain and the acoustic domain, respectively, $\boldsymbol{H}$ is the system coupling matrix and $\boldsymbol{f}_s$ is the external load on the structure.

In the component mode synthesis (CMS) method, the vibration equations of the subcomponents need to be transformed into modal coordinates through orthogonal normalization conditions. The matrix of the above coupled system equation is asymmetric, which will cause the system to generate complex modes when the subcomponents are synthesized. In addition, the left eigenvector and right eigenvector of the asymmetric coupling equation are not equal, so the eigenvector needs to be calculated twice, which increases the amount of calculation. Therefore, before the modal synthesis, the equation needs to be symmetric. The symmetric processing method in [21] has disadvantages such as matrix singularity and matrix dimension expansion, which are disadvantageous to solve the eigenmatrix of the system. The symmetric method in [22, 23] requires the inverse of the acoustic stiffness matrix, and in order to adapt to natural boundary conditions, complex frequency shift processing and modal inverse transformation processing are required. To deal with these disadvantages, this paper proposes the following symmetric method. From Eq. (1), the expression is as follows:

$$\begin{cases} \boldsymbol{M}_s \ddot{\boldsymbol{u}}_s + \rho \boldsymbol{H} \ddot{\boldsymbol{\psi}}_f + \boldsymbol{K}_s \boldsymbol{u}_s = \boldsymbol{f}_s \\ \boldsymbol{M}_f \ddot{\boldsymbol{\psi}}_f = c^2 \boldsymbol{H}^T \boldsymbol{u}_s - \boldsymbol{K}_f \boldsymbol{\psi}_f \end{cases} \tag{2}$$

Substituting the second formula of Eq. (2) into Eq. (1), and simultaneously multiplying the two ends of the second formula in Eq. (1) by $\left(\rho_f \boldsymbol{K}_f \boldsymbol{M}_f^{-1} / c^2\right)$, we can obtain the following equations:

$$\begin{cases} \boldsymbol{M}_s \ddot{\boldsymbol{u}}_s + \left(c^2 \rho_f \boldsymbol{H} \boldsymbol{M}_f^{-1} \boldsymbol{H}^T + \boldsymbol{K}_s\right) \boldsymbol{u}_s - \rho_f \boldsymbol{H} \boldsymbol{M}_f^{-1} \boldsymbol{K}_f \boldsymbol{\psi}_f = \boldsymbol{f}_s \\ \frac{\rho_f \boldsymbol{K}_f}{c^2} \ddot{\boldsymbol{\psi}}_f - \rho_f \boldsymbol{K}_f \boldsymbol{M}_f^{-1} \boldsymbol{H}^T \boldsymbol{u}_s + \rho_f \boldsymbol{K}_f \boldsymbol{M}_f^{-1} \boldsymbol{K}_f \boldsymbol{\psi}_f = \boldsymbol{0} \end{cases} \tag{3}$$

Then, we can get the symmetric vibration-acoustic coupling equation

$$\begin{bmatrix} \boldsymbol{M}_s & \boldsymbol{0} \\ \boldsymbol{0} & \tilde{\boldsymbol{M}}_f \end{bmatrix} \begin{bmatrix} \ddot{\boldsymbol{u}}_s \\ \ddot{\boldsymbol{\psi}}_f \end{bmatrix} + \begin{bmatrix} \tilde{\boldsymbol{K}}_s & -\tilde{\boldsymbol{H}} \\ -\tilde{\boldsymbol{H}}^T & \tilde{\boldsymbol{K}}_f \end{bmatrix} \begin{bmatrix} \boldsymbol{u}_s \\ \boldsymbol{\psi}_f \end{bmatrix} = \begin{bmatrix} \boldsymbol{f}_s \\ \boldsymbol{0} \end{bmatrix} \tag{4}$$

where

$$\begin{cases} \tilde{\boldsymbol{M}}_{\mathrm{f}} = \dfrac{\rho_{\mathrm{f}}\boldsymbol{K}_{\mathrm{f}}}{c^2} \\ \tilde{\boldsymbol{K}}_{\mathrm{s}} = c^2\rho_{\mathrm{f}}\boldsymbol{H}\boldsymbol{M}_{\mathrm{f}}^{-1}\boldsymbol{H}^{\mathrm{T}} + \boldsymbol{K}_{\mathrm{s}} \\ \tilde{\boldsymbol{K}}_{\mathrm{f}} = \dfrac{\rho_{\mathrm{f}}\boldsymbol{K}_{\mathrm{f}}\boldsymbol{M}_{\mathrm{f}}^{-1}\boldsymbol{K}_{\mathrm{f}}}{c^2} \\ \tilde{\boldsymbol{H}} = \rho_{\mathrm{f}}\boldsymbol{H}\boldsymbol{M}_{\mathrm{f}}^{-1}\boldsymbol{K}_{\mathrm{f}} \end{cases} \tag{5}$$

For the frequency response analysis, the response is time independent. The fluid displacement potential and the structural displacement response both conform to the form of $A = \|A\| \exp(-i\omega t)$; then, Eq. (4) is converted into the frequency form as

$$\left(\begin{bmatrix} \tilde{\boldsymbol{K}}_{\mathrm{s}} & -\tilde{\boldsymbol{H}} \\ -\tilde{\boldsymbol{H}}^{\mathrm{T}} & \tilde{\boldsymbol{K}}_{\mathrm{f}} \end{bmatrix} - \omega^2 \begin{bmatrix} \boldsymbol{M}_{\mathrm{s}} & \boldsymbol{0} \\ \boldsymbol{0} & \tilde{\boldsymbol{M}}_{\mathrm{f}} \end{bmatrix} \right) \begin{bmatrix} \boldsymbol{u}_{\mathrm{s}} \\ \boldsymbol{\psi}_{\mathrm{f}} \end{bmatrix} = \begin{bmatrix} \boldsymbol{f}_{\mathrm{s}} \\ \boldsymbol{0} \end{bmatrix} \tag{6}$$

where ω is the angular frequency of the external harmonic excitation. The above equation can be used to obtain the structural displacement u_{s} and the fluid displacement potential ψ_{f}, and the sound pressure can be obtained from the relationship between the fluid sound pressure p_{f} and the fluid displacement potential ψ_{f} as follows:

$$p_{\mathrm{f}} = -\rho_{\mathrm{f}}\omega^2\psi_{\mathrm{f}} \tag{7}$$

The response of a coupled system can generally be solved by the modal superposition method. However, the modal superposition method is not applicable to nonzero displacement boundary problems or nonzero pressure boundary problems. These problems are applicable to the direct method. After matrix symmetrization, the left eigenvector and right eigenvector of the coupled equation are the same. Therefore, the response can be directly calculated using the modal superposition method. The following equation is the modal superposition method of the acoustic vibration coupling system under the excitation of harmonic excitation:

$$\boldsymbol{X} = \sum_{i=1}^{N} \frac{[\boldsymbol{\varphi}_i][\boldsymbol{\varphi}_i]^{\mathrm{T}}}{\lambda_i - \omega^2}\boldsymbol{f} \tag{8}$$

where $\boldsymbol{\varphi}_i$ is the ith eigenvector of the coupled system, $\boldsymbol{f}$ is the external load.

2.2 Mode Synthesis of Structure-Acoustic Coupling System

In acoustic optimization problems, only part of the structure needs to be modified, and the rest remains unchanged. Therefore, the coupling system can be divided into two substructures along a boundary in the structural domain, and the division interface is set in the structural domain. This can satisfy the compatibilities for both displacement and force on the division interface. In this part, component A is a structural part, and component B is a vibro-acoustic coupling system composed of a partial structure and the whole acoustic domain.

To clearly show the relationship between the subcomponents and the DOFs of the interface, Fig. 1 shows a simple schematic diagram of an interface between two components. The structural domain of the full model is composed of four structural elements, and the acoustic domain is composed of two acoustic elements. The component A is composed of two structural elements, and the component B is composed of two structural elements and two acoustic elements. In the 2D problem, each structural node has two DOFs, and each acoustic node has one DOF. The structural DOFs or acoustic DOFs corresponding to the node are shown in brackets.

After dividing into two substructures on the division interface, the 7–12 DOFs of component A are interface DOFs, and the 1–6 degrees of freedom of substructure B are interface DOFs. The interface force $\boldsymbol{f}_{\mathrm{j}}$ is applied to the interface DOFs of the two components, and the magnitudes are equal and the directions are opposite. It should be noted that when calculating the eigenvalues and eigenvectors of substructures, the interface degrees of freedom of the two substructures need to be constrained.

Suppose there is no external load, only the interface force. The DOFs are separated into interface DOFs with index j and free DOFs denoted by index i. The vibration equations of subcomponent A and subcomponent B are as follows:

$$\begin{bmatrix} \boldsymbol{M}_{\mathrm{s,ii}}^{\mathrm{A}} & \boldsymbol{M}_{\mathrm{s,ij}}^{\mathrm{A}} \\ \boldsymbol{M}_{\mathrm{s,ji}}^{\mathrm{A}} & \boldsymbol{M}_{\mathrm{s,jj}}^{\mathrm{A}} \end{bmatrix} \begin{bmatrix} \ddot{\boldsymbol{u}}_{\mathrm{s,i}}^{\mathrm{A}} \\ \ddot{\boldsymbol{u}}_{\mathrm{s,j}}^{\mathrm{A}} \end{bmatrix} + \begin{bmatrix} \boldsymbol{K}_{\mathrm{s,ii}}^{\mathrm{A}} & \boldsymbol{K}_{\mathrm{s,ij}}^{\mathrm{A}} \\ \boldsymbol{K}_{\mathrm{s,ji}}^{\mathrm{A}} & \boldsymbol{K}_{\mathrm{s,jj}}^{\mathrm{A}} \end{bmatrix} \begin{bmatrix} \boldsymbol{u}_{\mathrm{s,i}}^{\mathrm{A}} \\ \boldsymbol{u}_{\mathrm{s,j}}^{\mathrm{A}} \end{bmatrix} = \begin{bmatrix} \boldsymbol{0} \\ \boldsymbol{f}_{\mathrm{j}}^{\mathrm{A}} \end{bmatrix} \tag{9}$$

$$\begin{bmatrix} \boldsymbol{M}_{\mathrm{s,jj}}^{\mathrm{B}} & \boldsymbol{M}_{\mathrm{s,ji}}^{\mathrm{B}} & \boldsymbol{0} \\ \boldsymbol{M}_{\mathrm{s,ij}}^{\mathrm{B}} & \boldsymbol{M}_{\mathrm{s,ii}}^{\mathrm{B}} & \boldsymbol{0} \\ \boldsymbol{0} & \boldsymbol{0} & \tilde{\boldsymbol{M}}_{\mathrm{f}} \end{bmatrix} \begin{bmatrix} \ddot{\boldsymbol{u}}_{\mathrm{s,j}}^{\mathrm{B}} \\ \ddot{\boldsymbol{u}}_{\mathrm{s,i}}^{\mathrm{B}} \\ \ddot{\boldsymbol{\psi}}_{\mathrm{f}} \end{bmatrix} + \begin{bmatrix} \tilde{\boldsymbol{K}}_{\mathrm{s,jj}}^{\mathrm{B}} & \tilde{\boldsymbol{K}}_{\mathrm{s,ji}}^{\mathrm{B}} & -\tilde{\boldsymbol{H}}_{\mathrm{j}} \\ \tilde{\boldsymbol{K}}_{\mathrm{s,ij}}^{\mathrm{B}} & \tilde{\boldsymbol{K}}_{\mathrm{s,ii}}^{\mathrm{B}} & -\tilde{\boldsymbol{H}}_{\mathrm{i}} \\ -\tilde{\boldsymbol{H}}_{\mathrm{j}}^{\mathrm{T}} & -\tilde{\boldsymbol{H}}_{\mathrm{i}}^{\mathrm{T}} & \tilde{\boldsymbol{K}}_{\mathrm{f}} \end{bmatrix} \begin{bmatrix} \boldsymbol{u}_{\mathrm{s,j}}^{\mathrm{B}} \\ \boldsymbol{u}_{\mathrm{s,i}}^{\mathrm{B}} \\ \boldsymbol{\psi}_{\mathrm{f}} \end{bmatrix} = \begin{bmatrix} \boldsymbol{f}_{\mathrm{j}}^{\mathrm{B}} \\ \boldsymbol{0} \\ \boldsymbol{0} \end{bmatrix} \tag{10}$$

where $\boldsymbol{f}_{\mathrm{j}}^{\mathrm{A}}$ and $\boldsymbol{f}_{\mathrm{j}}^{\mathrm{B}}$ are the force on the interface. Superscripts A and B are used to distinguish subcomponents A and B

For Craig–Bampton method, the interface DOFs are fixed, and the free vibration equation of the subcomponent can be obtained as follows:

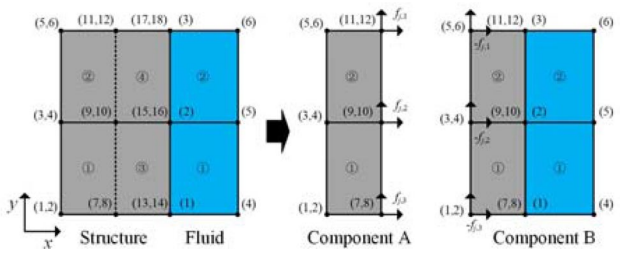

Fig. 1 Schematic diagram of an interface between two components

$$\boldsymbol{M}_{\mathrm{s,ii}}^{\mathrm{A}}\ddot{\boldsymbol{u}}_{\mathrm{s,i}}^{\mathrm{A}}+\boldsymbol{K}_{\mathrm{s,ii}}^{\mathrm{A}}\boldsymbol{u}_{\mathrm{s,i}}^{\mathrm{A}}=\boldsymbol{0} \tag{11}$$

$$\begin{bmatrix}\boldsymbol{M}_{\mathrm{s,ii}}^{\mathrm{B}} & \boldsymbol{0}\\ \boldsymbol{0} & \tilde{\boldsymbol{M}}_{\mathrm{f}}\end{bmatrix}\begin{bmatrix}\ddot{\boldsymbol{u}}_{\mathrm{s,i}}^{\mathrm{B}}\\ \ddot{\boldsymbol{\psi}}_{\mathrm{f}}\end{bmatrix}+\begin{bmatrix}\tilde{\boldsymbol{K}}_{\mathrm{s,ii}}^{\mathrm{B}} & -\tilde{\boldsymbol{H}}_{\mathrm{i}}\\ -\tilde{\boldsymbol{H}}_{\mathrm{i}}^{\mathrm{T}} & \tilde{\boldsymbol{K}}_{\mathrm{f}}\end{bmatrix}\begin{bmatrix}\boldsymbol{u}_{\mathrm{s,i}}^{\mathrm{B}}\\ \boldsymbol{\psi}_{\mathrm{f}}\end{bmatrix}=\begin{bmatrix}\boldsymbol{0}\\ \boldsymbol{0}\end{bmatrix} \tag{12}$$

The symmetrical form of the coupling equation satisfies the normalization condition

$$\begin{cases}\left(\boldsymbol{\varphi}_{\mathrm{ii}}^{\mathrm{A}}\right)^{\mathrm{T}}\boldsymbol{M}_{\mathrm{s,ii}}^{\mathrm{A}}\boldsymbol{\varphi}_{\mathrm{ii}}^{\mathrm{A}}=\boldsymbol{I}\\ \left(\boldsymbol{\varphi}_{\mathrm{ii}}^{\mathrm{A}}\right)^{\mathrm{T}}\boldsymbol{K}_{\mathrm{s,ii}}^{\mathrm{A}}\boldsymbol{\varphi}_{\mathrm{ii}}^{\mathrm{A}}=\lambda_{\mathrm{A}}^{2}\end{cases} \tag{13}$$

$$\begin{cases}\left(\boldsymbol{\varphi}_{\mathrm{ii}}^{\mathrm{B}}\right)^{\mathrm{T}}\begin{bmatrix}\boldsymbol{M}_{\mathrm{s,ii}}^{\mathrm{B}} & \boldsymbol{0}\\ \boldsymbol{0} & \tilde{\boldsymbol{M}}_{\mathrm{f}}\end{bmatrix}\boldsymbol{\varphi}_{\mathrm{ii}}^{\mathrm{B}}=\boldsymbol{I}\\ \left(\boldsymbol{\varphi}_{\mathrm{ii}}^{\mathrm{B}}\right)^{\mathrm{T}}\begin{bmatrix}\tilde{\boldsymbol{K}}_{\mathrm{s,ii}}^{\mathrm{B}} & -\tilde{\boldsymbol{H}}_{\mathrm{i}}\\ -\tilde{\boldsymbol{H}}_{\mathrm{i}}^{\mathrm{T}} & \tilde{\boldsymbol{K}}_{\mathrm{f}}\end{bmatrix}\boldsymbol{\varphi}_{\mathrm{ii}}^{\mathrm{B}}=\lambda_{\mathrm{B}}^{2}\end{cases} \tag{14}$$

where $\mathbf{I}$ is unit diagonal matrix. $\boldsymbol{\varphi}_{\mathrm{ii}}^{\mathrm{A}}$ and $\boldsymbol{\varphi}_{\mathrm{ii}}^{\mathrm{B}}$ are the main mode matrix of two subcomponents, respectively. $\boldsymbol{\lambda}$ is a diagonal matrix composed of eigenvalues.

There is only the main mode in the above equations, and discarding the higher-order mode will produce a larger error. The method of introducing interface constraint mode is adopted to reduce the error in Craig–Bampton method. Ignoring the inertial force, the following equation can be obtained from Eq. (9)

$$\boldsymbol{\varphi}_{\mathrm{r}}^{\mathrm{A}}=-\left(\boldsymbol{K}_{\mathrm{s,ii}}^{\mathrm{A}}\right)^{-1}\boldsymbol{K}_{\mathrm{s,ij}}^{\mathrm{A}} \tag{15}$$

Component B is a coupled system, and the constrained modes in the acoustic domain need to be calculated. Similarly, the constraint mode is obtained by ignoring the inertia force, which is obtained by Eq. (10)

$$\begin{bmatrix}\tilde{\boldsymbol{K}}_{\mathrm{s,jj}}^{\mathrm{B}} & \tilde{\boldsymbol{K}}_{\mathrm{s,ji}}^{\mathrm{B}} & -\tilde{\boldsymbol{H}}_{\mathrm{j}}\\ \tilde{\boldsymbol{K}}_{\mathrm{s,ij}}^{\mathrm{B}} & \tilde{\boldsymbol{K}}_{\mathrm{s,ii}}^{\mathrm{B}} & -\tilde{\boldsymbol{H}}_{\mathrm{i}}\\ -\tilde{\boldsymbol{H}}_{\mathrm{j}}^{\mathrm{T}} & -\tilde{\boldsymbol{H}}_{\mathrm{i}}^{\mathrm{T}} & \tilde{\boldsymbol{K}}_{\mathrm{f}}\end{bmatrix}\begin{bmatrix}\boldsymbol{I}\\ \boldsymbol{\varphi}_{2}^{\mathrm{B}}\\ \boldsymbol{\varphi}_{1}^{\mathrm{B}}\end{bmatrix}=\begin{bmatrix}\boldsymbol{R}_{\mathrm{c}}\\ \boldsymbol{0}\\ \boldsymbol{0}\end{bmatrix} \tag{16}$$

where $\boldsymbol{R}_{\mathrm{c}}$ is the interface force under unit displacement. $\boldsymbol{\varphi}_{1}^{\mathrm{B}}$ and $\boldsymbol{\varphi}_{2}^{\mathrm{B}}$ are the constrained modes of component B. The following formulas are obtained

$$\boldsymbol{\varphi}_{1}^{\mathrm{B}}=\left(\tilde{\boldsymbol{K}}_{\mathrm{f}}-\tilde{\boldsymbol{H}}_{\mathrm{j}}^{\mathrm{T}}\left(\tilde{\boldsymbol{K}}_{\mathrm{s,ii}}^{\mathrm{B}}\right)^{-1}\tilde{\boldsymbol{H}}_{\mathrm{i}}\right)^{-1}\left(\tilde{\boldsymbol{H}}_{\mathrm{j}}^{\mathrm{T}}-\tilde{\boldsymbol{H}}_{\mathrm{i}}^{\mathrm{T}}\left(\tilde{\boldsymbol{K}}_{\mathrm{s,ii}}^{\mathrm{B}}\right)^{-1}\tilde{\boldsymbol{K}}_{\mathrm{s,ij}}^{\mathrm{B}}\right) \tag{17}$$

$$\boldsymbol{\varphi}_{2}^{\mathrm{B}}=\left(\tilde{\boldsymbol{K}}_{\mathrm{s,ii}}^{\mathrm{B}}\right)^{-1}\begin{pmatrix}\tilde{\boldsymbol{H}}_{\mathrm{i}}\left(\tilde{\boldsymbol{K}}_{\mathrm{f}}-\tilde{\boldsymbol{H}}_{\mathrm{j}}^{\mathrm{T}}\left(\tilde{\boldsymbol{K}}_{\mathrm{s,ii}}^{\mathrm{B}}\right)^{-1}\tilde{\boldsymbol{H}}_{\mathrm{i}}\right)^{-1}\times\\ \left(\tilde{\boldsymbol{H}}_{\mathrm{j}}^{\mathrm{T}}-\tilde{\boldsymbol{H}}_{\mathrm{i}}^{\mathrm{T}}\left(\tilde{\boldsymbol{K}}_{\mathrm{s,ii}}^{\mathrm{B}}\right)^{-1}\tilde{\boldsymbol{K}}_{\mathrm{s,ij}}^{\mathrm{B}}\right)\\ -\tilde{\boldsymbol{K}}_{\mathrm{s,ij}}^{\mathrm{B}}\end{pmatrix} \tag{18}$$

$$\boldsymbol{\varphi}_{\mathrm{r}}^{\mathrm{B}}=\begin{bmatrix}\boldsymbol{\varphi}_{2}^{\mathrm{B}}\\ \boldsymbol{\varphi}_{1}^{\mathrm{B}}\end{bmatrix} \tag{19}$$

The interface constraint mode is added to the main mode, and then the component mode set $\boldsymbol{\varphi}_{\mathrm{c}}^{\mathrm{A}}$ and $\boldsymbol{\varphi}_{\mathrm{c}}^{\mathrm{B}}$ can be obtained

$$\begin{cases}\boldsymbol{\varphi}_{\mathrm{c}}^{\mathrm{A}}=\begin{bmatrix}\boldsymbol{\varphi}_{\mathrm{ii}}^{\mathrm{A}} & \boldsymbol{\varphi}_{\mathrm{r}}^{\mathrm{A}}\\ \boldsymbol{0} & \mathbf{I}\end{bmatrix}\\ \boldsymbol{\varphi}_{\mathrm{c}}^{\mathrm{B}}=\begin{bmatrix}\boldsymbol{\varphi}_{\mathrm{ii}}^{\mathrm{B}} & \boldsymbol{\varphi}_{\mathrm{r}}^{\mathrm{B}}\\ \boldsymbol{0} & \mathbf{I}\end{bmatrix}\end{cases} \tag{20}$$

According to the relationship between physical coordinates and modal coordinates,

$$\begin{cases}\begin{bmatrix}\boldsymbol{u}_{\mathrm{s,i}}^{\mathrm{A}}\\ \boldsymbol{u}_{\mathrm{s,j}}^{\mathrm{A}}\end{bmatrix}=\boldsymbol{\varphi}_{\mathrm{c}}^{\mathrm{A}}\boldsymbol{p}^{\mathrm{A}}=\begin{bmatrix}\boldsymbol{\varphi}_{\mathrm{ii}}^{\mathrm{A}} & \boldsymbol{\varphi}_{\mathrm{r}}^{\mathrm{A}}\\ \boldsymbol{0} & \mathbf{I}\end{bmatrix}\begin{bmatrix}\boldsymbol{p}_{\mathrm{i}}^{\mathrm{A}}\\ \boldsymbol{p}_{\mathrm{j}}^{\mathrm{A}}\end{bmatrix}\\ \begin{bmatrix}\boldsymbol{u}_{\mathrm{s,i}}^{\mathrm{B}}\\ \boldsymbol{u}_{\mathrm{s,j}}^{\mathrm{B}}\\ \boldsymbol{\psi}_{\mathrm{f}}\end{bmatrix}=\boldsymbol{\varphi}_{\mathrm{c}}^{\mathrm{B}}\boldsymbol{p}^{\mathrm{B}}=\begin{bmatrix}\boldsymbol{\varphi}_{\mathrm{ii}}^{\mathrm{B}} & \boldsymbol{\varphi}_{\mathrm{r}}^{\mathrm{B}}\\ \boldsymbol{0} & \mathbf{I}\end{bmatrix}\begin{bmatrix}\boldsymbol{p}_{\mathrm{i}}^{\mathrm{B}}\\ \boldsymbol{p}_{\mathrm{j}}^{\mathrm{B}}\end{bmatrix}\end{cases} \tag{21}$$

where $\boldsymbol{p}^{\mathrm{A}}$ and $\boldsymbol{p}^{\mathrm{B}}$ are the generalized coordinates of subcomponents A and B, respectively.

By substituting the above equation into the vibration equation of components A and B, we can obtain the modal coordinate form of the vibration equation of these two components

$$\begin{cases}\bar{\boldsymbol{M}}^{\mathrm{A}}\ddot{\boldsymbol{p}}^{\mathrm{A}}+\bar{\boldsymbol{K}}^{\mathrm{A}}\boldsymbol{p}^{\mathrm{A}}=\begin{bmatrix}\boldsymbol{0}\\ \boldsymbol{f}_{\mathrm{j}}^{\mathrm{A}}\end{bmatrix}\\ \bar{\boldsymbol{M}}^{\mathrm{B}}\ddot{\boldsymbol{p}}^{\mathrm{B}}+\bar{\boldsymbol{K}}^{\mathrm{B}}\boldsymbol{p}^{\mathrm{B}}=\begin{bmatrix}\boldsymbol{0}\\ \boldsymbol{f}_{\mathrm{j}}^{\mathrm{B}}\end{bmatrix}\end{cases} \tag{22}$$

where

$$\begin{cases}\bar{\boldsymbol{M}}^{\mathrm{A}}=\left(\boldsymbol{\varphi}_{\mathrm{c}}^{\mathrm{A}}\right)^{\mathrm{T}}\begin{bmatrix}\boldsymbol{M}_{\mathrm{s,ii}}^{\mathrm{A}} & \boldsymbol{M}_{\mathrm{s,ij}}^{\mathrm{A}}\\ \boldsymbol{M}_{\mathrm{s,ji}}^{\mathrm{A}} & \boldsymbol{M}_{\mathrm{s,jj}}^{\mathrm{A}}\end{bmatrix}\boldsymbol{\varphi}_{\mathrm{c}}^{\mathrm{A}}\\ \bar{\boldsymbol{K}}^{\mathrm{A}}=\left(\boldsymbol{\varphi}_{\mathrm{c}}^{\mathrm{A}}\right)^{\mathrm{T}}\begin{bmatrix}\boldsymbol{K}_{\mathrm{s,ii}}^{\mathrm{A}} & \boldsymbol{K}_{\mathrm{s,ij}}^{\mathrm{A}}\\ \boldsymbol{K}_{\mathrm{s,ji}}^{\mathrm{A}} & \boldsymbol{K}_{\mathrm{s,jj}}^{\mathrm{A}}\end{bmatrix}\boldsymbol{\varphi}_{\mathrm{c}}^{\mathrm{A}}\end{cases} \tag{23}$$

$$\begin{cases} \bar{\boldsymbol{M}}^{\mathrm{B}} = \left(\boldsymbol{\varphi}_{\mathrm{c}}^{\mathrm{B}}\right)^{\mathrm{T}} \begin{bmatrix} \boldsymbol{M}_{\mathrm{s,jj}}^{\mathrm{B}} & \boldsymbol{M}_{\mathrm{s,ji}}^{\mathrm{B}} & \boldsymbol{0} \\ \boldsymbol{M}_{\mathrm{s,ij}}^{\mathrm{B}} & \boldsymbol{M}_{\mathrm{s,ii}}^{\mathrm{B}} & \boldsymbol{0} \\ \boldsymbol{0} & \boldsymbol{0} & \tilde{\boldsymbol{M}}_{\mathrm{f}} \end{bmatrix} \boldsymbol{\varphi}_{\mathrm{c}}^{\mathrm{B}} \\ \bar{\boldsymbol{K}}^{\mathrm{B}} = \left(\boldsymbol{\varphi}_{\mathrm{c}}^{\mathrm{B}}\right)^{\mathrm{T}} \begin{bmatrix} \tilde{\boldsymbol{K}}_{\mathrm{s,jj}}^{\mathrm{B}} & \tilde{\boldsymbol{K}}_{\mathrm{s,ji}}^{\mathrm{B}} & -\tilde{\boldsymbol{H}}_{\mathrm{j}} \\ \tilde{\boldsymbol{K}}_{\mathrm{s,ij}}^{\mathrm{B}} & \tilde{\boldsymbol{K}}_{\mathrm{s,ii}}^{\mathrm{B}} & -\tilde{\boldsymbol{H}}_{\mathrm{i}} \\ -\tilde{\boldsymbol{H}}_{\mathrm{j}}^{\mathrm{T}} & -\tilde{\boldsymbol{H}}_{\mathrm{i}}^{\mathrm{T}} & \tilde{\boldsymbol{K}}_{\mathrm{f}} \end{bmatrix} \boldsymbol{\varphi}_{\mathrm{c}}^{\mathrm{B}} \end{cases} \tag{24}$$

To form the vibration equation of the whole system, the vibration equation of each component needs to be synthesized. According to the displacement and force continuity conditions between interfaces, the interface modal coordinates of component A and B are the same

$$\boldsymbol{p}_{\mathrm{j}}^{\mathrm{A}} = \boldsymbol{p}_{\mathrm{j}}^{\mathrm{B}} \tag{25}$$

Formulas of generalized coordinates and modal coordinates are as follows:

$$\boldsymbol{p} = \begin{bmatrix} \boldsymbol{p}_{\mathrm{i}}^{\mathrm{A}} \\ \boldsymbol{p}_{\mathrm{j}}^{\mathrm{A}} \\ \boldsymbol{p}_{\mathrm{i}}^{\mathrm{B}} \\ \boldsymbol{p}_{\mathrm{j}}^{\mathrm{B}} \end{bmatrix} = \begin{bmatrix} \mathbf{I00} \\ \mathbf{00I} \\ \mathbf{0I0} \\ \mathbf{00I} \end{bmatrix} \begin{bmatrix} \boldsymbol{q}_{\mathrm{i}}^{\mathrm{A}} \\ \boldsymbol{q}_{\mathrm{i}}^{\mathrm{B}} \\ \boldsymbol{q}_{\mathrm{j}} \end{bmatrix} = \boldsymbol{T}\boldsymbol{q} \tag{26}$$

where $\boldsymbol{q}$ is generalized coordinate.

The vibration equations of components A and B in modal coordinates are as follows:

$$\bar{\boldsymbol{M}}^{\mathrm{A}} \begin{bmatrix} \ddot{\boldsymbol{p}}_{\mathrm{i}}^{\mathrm{A}} \\ \ddot{\boldsymbol{p}}_{\mathrm{j}}^{\mathrm{A}} \end{bmatrix} + \bar{\boldsymbol{K}}^{\mathrm{A}} \begin{bmatrix} \boldsymbol{p}_{\mathrm{i}}^{\mathrm{A}} \\ \boldsymbol{p}_{\mathrm{j}}^{\mathrm{A}} \end{bmatrix} = \begin{bmatrix} \boldsymbol{0} \\ \boldsymbol{f}_{\mathrm{j}}^{\mathrm{A}} \end{bmatrix} \tag{27}$$

$$\bar{\boldsymbol{M}}^{\mathrm{B}} \begin{bmatrix} \ddot{\boldsymbol{p}}_{\mathrm{j}}^{\mathrm{B}} \\ \ddot{\boldsymbol{p}}_{\mathrm{j}}^{\mathrm{B}} \end{bmatrix} + \bar{\boldsymbol{K}}^{\mathrm{B}} \begin{bmatrix} \boldsymbol{p}_{\mathrm{j}}^{\mathrm{B}} \\ \boldsymbol{p}_{\mathrm{j}}^{\mathrm{B}} \end{bmatrix} = \begin{bmatrix} \boldsymbol{0} \\ \boldsymbol{f}_{\mathrm{j}}^{\mathrm{B}} \end{bmatrix} \tag{28}$$

The relationship between interface forces is $\boldsymbol{f}_{\mathrm{j}}^{\mathrm{A}} = -\boldsymbol{f}_{\mathrm{j}}^{\mathrm{B}}$. The free vibration equation after mode synthesis is obtained by the transposition of Eq. (26) to Eq. (28) and premultiplied by $\boldsymbol{T}^{\mathrm{T}}$

$$\boldsymbol{M}\ddot{\boldsymbol{q}} + \boldsymbol{K}\boldsymbol{q} = \boldsymbol{0} \tag{29}$$

where

$$\begin{cases} \boldsymbol{M} = \boldsymbol{T}^{\mathrm{T}} \begin{bmatrix} \bar{\boldsymbol{M}}^{\mathrm{A}} \boldsymbol{0} \\ \boldsymbol{0} \bar{\boldsymbol{M}}^{\mathrm{B}} \end{bmatrix} \boldsymbol{T} \\ \boldsymbol{K} = \boldsymbol{T}^{\mathrm{T}} \begin{bmatrix} \bar{\boldsymbol{K}}^{\mathrm{A}} \boldsymbol{0} \\ \boldsymbol{0} \bar{\boldsymbol{K}}^{\mathrm{B}} \end{bmatrix} \boldsymbol{T} \end{cases} \tag{30}$$

The vibration in generalized coordinates is obtained by solving Eq. (29), so it needs to be restored to physical coordinates. The method is shown in the following equation

$$\begin{cases} \boldsymbol{u}^{\mathrm{A}} = \boldsymbol{\varphi}_{\mathrm{c}}^{\mathrm{A}} \boldsymbol{T}^{\mathrm{A}} \boldsymbol{q}^{\mathrm{A}} \\ \boldsymbol{u}^{\mathrm{B}} = \boldsymbol{\varphi}_{\mathrm{c}}^{\mathrm{B}} \boldsymbol{T}^{\mathrm{B}} \boldsymbol{q}^{\mathrm{B}} \end{cases} \tag{31}$$

where

$$\begin{cases} \boldsymbol{T}^{\mathrm{A}} = \begin{bmatrix} \mathbf{I} & \mathbf{0} & \mathbf{0} \\ \mathbf{0} & \mathbf{0} & \mathbf{I} \end{bmatrix} \\ \boldsymbol{T}^{\mathrm{B}} = \begin{bmatrix} \mathbf{0} & \mathbf{I} & \mathbf{0} \\ \mathbf{0} & \mathbf{0} & \mathbf{I} \end{bmatrix} \end{cases} \tag{32}$$

$$\begin{cases} \boldsymbol{q}^{\mathrm{A}} = \begin{bmatrix} \boldsymbol{q}_{\mathrm{i}}^{\mathrm{A}} \\ \boldsymbol{q}_{\mathrm{j}} \end{bmatrix} \\ \boldsymbol{q}^{\mathrm{B}} = \begin{bmatrix} \boldsymbol{q}_{\mathrm{i}}^{\mathrm{B}} \\ \boldsymbol{q}_{\mathrm{j}} \end{bmatrix} \end{cases} \tag{33}$$

Through the above model reduction method, the eigenvalue and eigenvector matrix can be obtained with a small calculation cost, and the response of the acoustic vibration coupling system under a given excitation can be obtained. Then, combined with the BESO topology optimization algorithm, the sensitivity analysis and noise reduction optimization are performed.

3 Element Sensitivity Analysis and Optimization Algorithm

3.1 Objective Function and Optimization Algorithm

The objective function and constraints of the optimal design for minimizing the system response are as follows:

$$\begin{cases} \min(C) \\ \text{s.t.} \quad V^* - \sum_{i=1}^{N} V_i x_i = 0,\ x_i \in \{x_{\min}, 1\} \end{cases} \tag{34}$$

where V^* is the prescribed final volume limit of the structure. x_i is the element design variable ($x_{\min}$ or 1).

The above objective is specified at a certain excitation frequency, but in practical, the external load is composed of a series of frequencies with different amplitudes, and the optimization result of the single-frequency excitation is not necessarily the optimal solution in the operating frequency range. In this part, all amplitudes are simplified to be the same, and for simplicity, the average excitation frequency of ω_1 to ω_2 is used as a new objective function:

$$C^0 = \frac{1}{\omega_2 - \omega_1} \int_{\omega_1}^{\omega_2} C d\omega \tag{35}$$

where ω_1 and ω_2 are the lower and upper frequency bounds, respectively. The objective function is derived from the element design variables

$$\frac{\partial C^0}{\partial x_i} = \frac{1}{\omega_2 - \omega_1} \int_{\omega_1}^{\omega_2} \frac{\partial C}{\partial x_i} d\omega \tag{36}$$

To avoid the local model of void parts in structure, an improved power rate penalty function (SIMP) model is needed to change the state variables to ensure the optimization results are more reasonable. In topology optimization algorithm, a radius-based filtering method and a historical average method of element sensitivity are needed to avoid "isolated grids" and accelerate convergence [24].

3.2 Sensitivity Analysis

Then, we use $\boldsymbol{K}_\mathrm{d}$ for the dynamic stiffness matrix on the left side of Eq. (6) and $\boldsymbol{f}$ for the external load on the right side of the equation:

$$\boldsymbol{K}_\mathrm{d}\boldsymbol{X} = \boldsymbol{f} \tag{37}$$

In practical applications, we only care about whether the value of the response becomes smaller, that is, the absolute value $\left|\boldsymbol{X}_j\right|$. Differentiating the design variable x_i with the response amplitude, we get

$$\frac{\partial \left|\boldsymbol{X}_j\right|}{\partial x_i} = \frac{\boldsymbol{X}_j}{\left|\boldsymbol{X}_j\right|} \frac{\partial \boldsymbol{X}_j}{\partial x_i} \tag{38}$$

The first term on the right side of the above equation can be directly obtained, and the second term is obtained by deriving x_i on the left and right sides of Eq. (37) and multiplying the adjoint vector $\boldsymbol{\Lambda}_j$ at the jth DOFs

$$\frac{\partial \boldsymbol{X}_j}{\partial x_i} = \boldsymbol{\Lambda}_j \frac{\partial \boldsymbol{X}}{\partial x_i} = \boldsymbol{\Lambda}_j \boldsymbol{K}_\mathrm{d}^{-1} \frac{\partial \boldsymbol{K}_\mathrm{d}}{\partial x_i} \boldsymbol{X} \tag{39}$$

Substituting the above equation into Eq. (38), we can get the sensitivity of the response amplitude at the jth DOF

$$\frac{\partial \left|\boldsymbol{X}_j\right|}{\partial x_i} = \frac{\boldsymbol{X}_j}{\left|\boldsymbol{X}_j\right|} \boldsymbol{\Lambda}_j \boldsymbol{K}_\mathrm{d}^{-1} \frac{\partial \boldsymbol{K}_\mathrm{d}}{\partial x_i} \boldsymbol{X} \tag{40}$$

The element sensitivity is the derivative of the element variable x_i. The derivative of dynamic stiffness $\boldsymbol{K}_\mathrm{d}$ to x_i in the above formula can be obtained from the penalty function model [24]:

$$\frac{\partial \boldsymbol{K}_\mathrm{d}}{\partial x_i} = \frac{1 - x_\mathrm{min}}{1 - x_\mathrm{min}^p} p x_i^{p-1} \boldsymbol{k}_i^\mathrm{e} - \omega^2 \boldsymbol{m}_i^\mathrm{e} \tag{41}$$

where $\boldsymbol{k}_i^\mathrm{e}$ and $\boldsymbol{m}_i^\mathrm{e}$ are the ith structural element stiffness matrix and element mass matrix, respectively. p is the penalty exponent factor. Thus, the element sensitivity is as follows:

$$\alpha_i = \frac{\boldsymbol{X}_j}{\left|\boldsymbol{X}_j\right|} \boldsymbol{\Lambda}_j^i \left(\boldsymbol{K}_\mathrm{d}^{-1}\right)^i \left(\frac{1 - x_\mathrm{min}}{1 - x_\mathrm{min}^p} p x_i^{p-1} \boldsymbol{k}_i^\mathrm{e} - \omega^2 \boldsymbol{m}_i^\mathrm{e} \right) \boldsymbol{X}^i \tag{42}$$

where α_i is the ith element sensitivity. The subscript i of the remaining variables represents the element corresponding to the degree of freedom of the ith element.

If $\boldsymbol{X}_j$ represents the fluid displacement potential, the sensitivity obtained by the above equation is the displacement potential sensitivity. It can be obtained from Eq. (7) that if the excitation frequency does not change, there is a linear relationship between fluid displacement potential and sound pressure. So the sensitivity Eq. (42) can also be used for sound pressure optimization.

4 Numerical Examples

4.1 Numerical Verification of the Vibro-Acoustic Mode Synthesis Method

In this part, the 2D vibro-acoustic system is shown in Fig. 2 with two components A and B which is divided along the split line. The computation domain with two subcomponents is discretized into linear four-node quadrilateral elements of size 0.01 m. The top of the acoustic domain is a boundary condition with zero sound pressure, and the rest of the walls are rigid boundaries. The bottom ends of the structure domain are fixed at both ends, and the specific dimensions are shown in

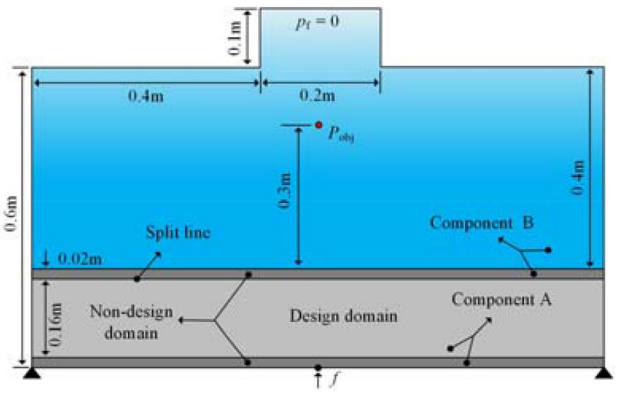

Fig. 2 Geometric properties and boundary conditions of a acoustic cavity system

the figure. The material properties of the structural domain are Young's modulus of 69 GPa, density of 2700 kg/m^3 and Poisson's ratio of 0.3. The acoustic domain has density of 1000 kg/m^3 and the speed of sound in the medium of 1450 m/s. The material properties of the following cases are the same as this example.

The system's number of DOFs directly determines the dimensions of the system matrix, which is related to the computer memory occupation and the amount of calculation. Table 1 shows the comparison of the DOFs in the calculation of eigenvalues and eigenvectors in the original system and the proposed model reduction method in this paper. The number of DOFs changes from 8593 to 602 with the method of mode synthesis. Although modal synthesis requires other processing steps, it still effectively reduces the amount of calculation. Table 2 gives the eigenvalues after modal synthesis and the full system. To ensure accuracy, the first 200 eigenvectors of each subcomponent are taken to participate in the mode synthesis. The relative errors between the first five orders of eigenvalues calculated by the proposed mode synthesis method and the overall calculation result of the original system are less than 0.005%.

Sound pressure level (SPL) is one of the important indicators to measure the accuracy of calculation results. A y-axis direction point load ($f = 1$N) is applied to the midpoint of the bottom of the structure domain shown in Fig. 2, and P_{obj} is the target point in the acoustic domain. The first 100 eigenvectors are taken to calculate system response in modal superposition method. Figure 3 shows the SPL values of the coupled system under direct method, mode superposition method without CMS method and mode superposition with CMS method. The objective value calculated by the direct method is almost similar to those of the mode superposition method of the full system and CMS method except in the low-frequency band. This is because the mode superposition method ignores the mode coupling effect when calculating acoustic radiation and generates a certain error.

The above content verifies the correctness of the response value and eigenvalue using the modal reduction method. Then, an optimization example is used to verify the effectiveness of the modal reduction method in optimization and the reduction in the amount of calculation. For this optimization example, the sound pressure level of point P_{obj} is set as the target with volume fraction of 50% under excitation frequency of 700 Hz. The filter radius is set to 0.02 m, the penalty factor is 3 and $x_{\min}$=0.0001.

Table 1 Comparison of DOFs for different models

	Component A	Component B	Interface	Full model	Mode synthesis
DOFs	3638	4957	202	8593	602

Table 2 Comparison of eigenvalue for origin method and mode synthesis method

Mode No.	1	2	3	4	5
Mode synthesis	260.35	648.03	695.95	899.21	1450.25
Full model	260.35	648.03	695.94	899.2	1450.18
Relative error	–	–	0.001%	0.001%	0.005%

The optimal designs of the two methods under the same conditions are shown in Fig. 4a, b. The structural topology of the two optimization results is almost the same. The modal reduction method only affects the response calculation results and time and has no effect on other steps in the optimization process, so only the time-consuming differences in the response calculation part are listed. The computing core of the computer used is AMD 3900X. It can be found from Fig. 4c that the iteration curve is stable, and there is almost no difference in the target value during the iteration of the two methods. Except for the first iteration step, in other iteration steps, the time consumed by the modal reduction method is significantly less than that without the modal reduction method. This is because the eigenvalues and eigenvectors of the two subcomponents need to be calculated separately in the first iteration. Since the subcomponent B does not change, only the eigenvalues and eigenvectors of the subcomponent A need to be calculated in the subsequent iteration steps, so the calculation time is reduced by an order of magnitude.

Figure 5 shows the target values of the optimal design and the initial design using the two methods. It can be found that the target values of the two optimized designs are almost the same. To reduce the target value, the curves of the target point shift to the right.

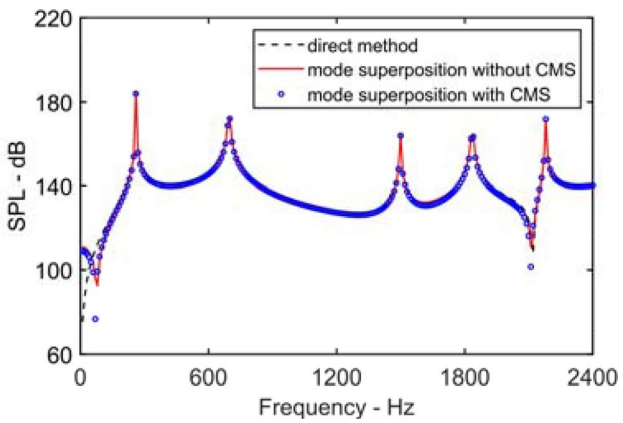

Fig. 3 Comparison of sound pressure level at the reference point under different excitation frequencies for three different methods

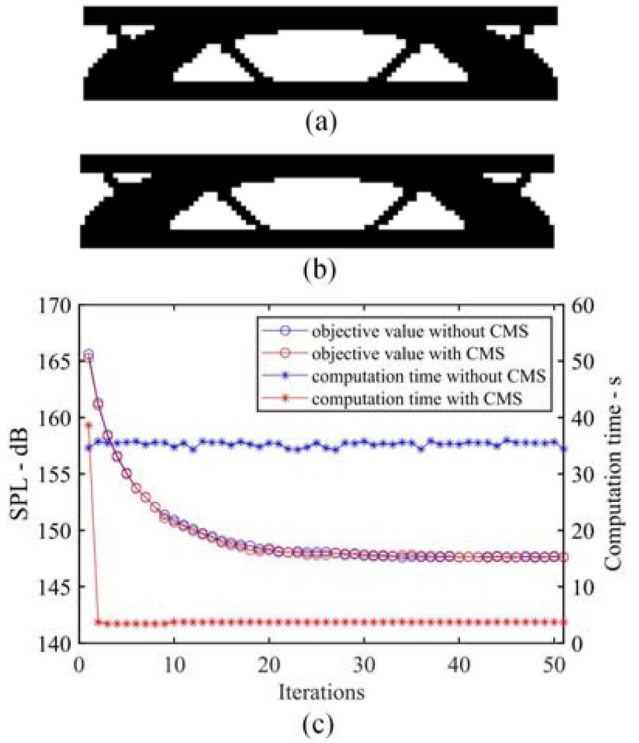

Fig. 4 Sound pressure minimization under same excitation frequency, **a** optimal design without CMS, **b** optimal design with CMS, **c** evolution histories of the objective function and computation time with different methods

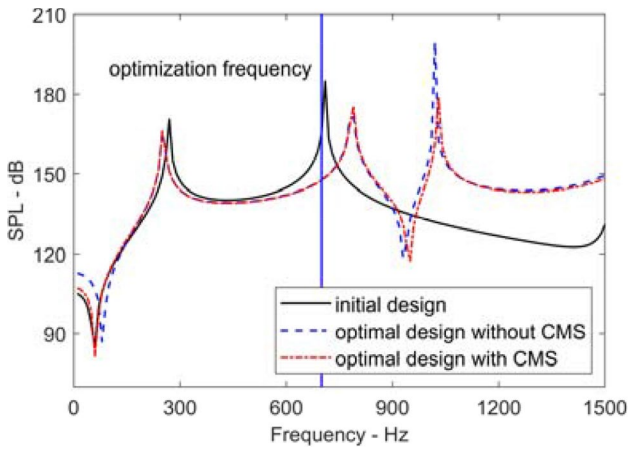

Fig. 5 Comparison of sound pressure level at the reference area under different excitation frequencies for the initial and the optimal design

4.2 Effect of Non-design Domain on Optimization Results

For this optimization example, a sound pressure minimization problem with two subcomponents in Fig. 6 is considered. Both sides of the structure are clamped, and the

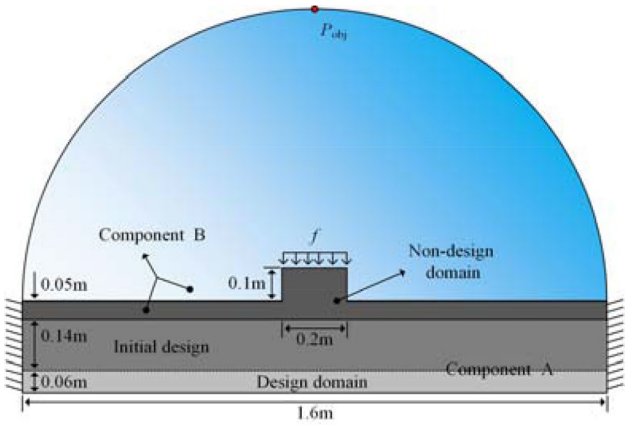

Fig. 6 Coupled system under a harmonic loading in the structure domain for minimization of the acoustic pressure at the top of the acoustic domain

boundaries of the acoustic domain are all rigid. Along the top of the design domain, the coupled system is divided into component A that changes with iteration and component B that does not change with iteration. In each optimization iteration step, it is only necessary to recalculate the eigenvalues and eigenvectors of the modified component A. After modal synthesis with the component B, the modified eigenvalues and eigenvectors of the entire system can be obtained, which greatly reduces the calculation.

To ensure the accuracy of the calculation and the smoothness at the optimized boundary, a discrete system of 0.01-m-sized elements is used. The filtering radius is set to two times the element size and the penalty factor is set to 3. The amplitude of the harmonic load is 1000 N at the top of the structure domain on each node, and the excitation frequency is set at 365 Hz. The objective is set to minimize the amplitude of the P_{obj} in the acoustic medium. To investigate the effect of the size of non-design domain on the final design. The first 200 modes of each component are taken for modal synthesis, and the mode superposition method takes the first 200 modes after modal synthesis for system response calculation.

In this optimization study, we keep the initial design domain at 78% of the entire structural domain and set three examples for different non-design domain sizes in Fig. 7. From the optimization results (a)–(g) of Fig. 8, it can be seen that whether the CMS method is adopted does not affect the topology of the optimized structure, but it effectively reduces the calculation time. The two methods have the same objective function value under the same boundary conditions. By comparing the optimization results of non-design domains with different sizes, it is found that the size of the non-design domains has a greater impact on the optimization results. From the response value of the target point, the larger the non-design domain, the larger the optimized

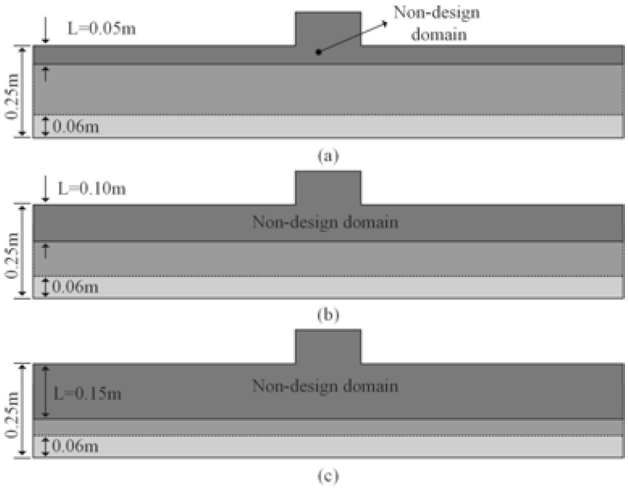

Fig. 7 Schematic diagram of different sizes of non-design domain. **a** $L=0.05$ m, **b** $L=0.10$ m, **c** $L=0.15$ m

target point sound pressure value. This shows that as the non-design domain increases, the optimization space also becomes smaller, and the final design cannot achieve the optimal results.

Table 3 shows the comparison of the DOFs of different models. The DOFs of the three models are greatly reduced. But this does not mean that the response calculation time is equal to the calculation time of the model after the modal reduction, because the modal synthesis method requires the eigenvalues and eigenvectors of each substructure.

Figure 9 shows the frequency response curve of the sound pressure level at the target point of the three examples before and after optimization. In order to facilitate the comparison of the optimization results of different non-design domain sizes, only the frequency response calculated by the CMS method is given in the figure. The peak frequencies of the three examples are 445 Hz, 440 Hz and 425 Hz. The larger the non-design domain is, the closer the peak frequency of the optimal design is to that of the original design, and the worse the optimization result is.

4.3 Multiobjective Optimization Example

The third optimization example investigates a clamped arched beam vibrating under an acoustic domain, which is shown in Fig. 10. A point load is imposed harmonically in the top of the beam with an amplitude of 100 N in the vertical direction. The objective function is set to minimize the sound pressure in the point of P_{obj} for a frequency range of the applied point load (176,186) Hz with a 60% volume constraint of the design domain. The internal thickness of the 0.15 m area is set as a non-design domain, and the initial design domain is 60% of the full design domain. Along the outer boundary of the design domain, the coupled system is divided into component A and component B. The first 300 modes of each component are taken for modal synthesis, and the first 200 modes after modal synthesis are taken for mode superposition method to calculate the system response.

As shown in the frequency response curve of Fig. 11, the system response resonance peak in the excitation frequency band has been moved to higher frequencies; that is, the resonance frequency has been increased. Under the same volume constraint, the optimization algorithm improves the coupling resonance by rationally arranging the material distribution. The target point sound pressure level is reduced from the initial 175.3 dB to 153.8 dB, a reduction of 12.3%. The frequency response curves of the two methods are similar to each other. Figure 12 shows the evolution histories of the objective function and computation time with different methods. In this example, although the iteration target values of the two methods are the same, the calculation time has not been effectively reduced. Table 3 explains that the response calculation time is equal to the calculation time of the model after the modal reduction, because the modal synthesis method requires the eigenvalues and eigenvectors of each substructure, especially this example, because the area of the component A is very large, and the component A changes in each iteration step. When performing modal synthesis, the eigenvalues and eigenvectors need to be recalculated. This shows that when the modal reduction method is applied to topology optimization, it has a better effect on problems with large nonvariable areas.

The contour plots for three designs at 186 Hz can be seen in Fig. 13. The optimized average sound pressure level of the target point is significantly smaller than the initial system. In addition, the vibration amplitude of both designs with or without the CMS method is greatly reduced, and the two designs are almost the same. This is because excitation frequency of the initial design is near the resonance frequency, and the optimized resonance frequency is far away from the excitation frequency range, so the structure amplitude is effectively reduced.

5 Conclusion

This paper presents a novel model reduction method based on the Craig–Bampton mode synthesis method and a newly proposed symmetric method of vibro-acoustic system matrix. This mode synthesis method can effectively reduce the DOFs of the coupled system. Furthermore, this method is applied to topology optimization of acoustic response that requires a large number of iterative calculations. Numerical optimization examples are performed, and the results show that:

The method of vibro-acoustic coupling mode synthesis proposed in this paper can effectively reduce the calculation

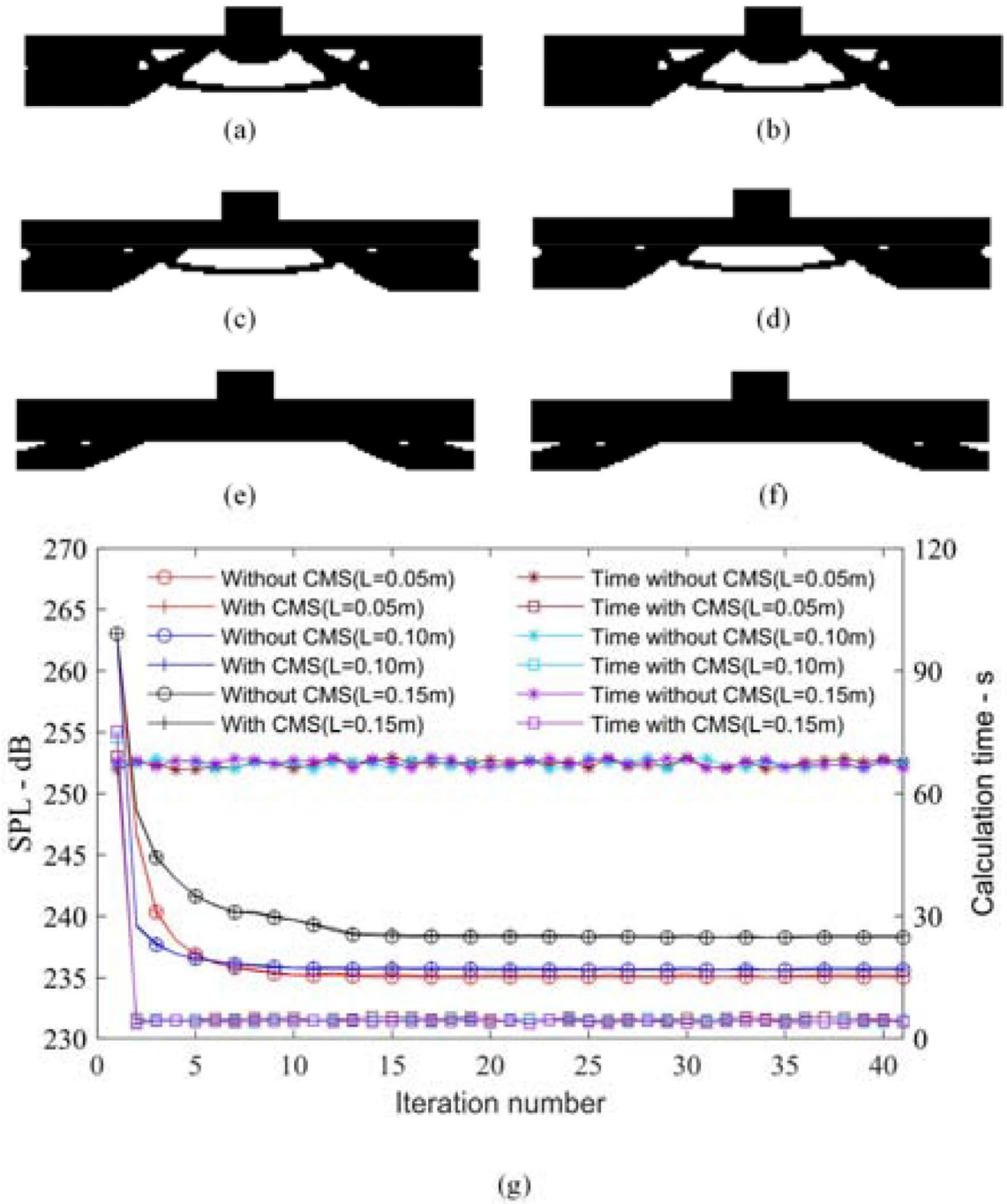

Fig. 8 Sound pressure minimization under same excitation frequency. **a** Optimal design without CMS(L = 0.05 m), **b** optimal design with CMS(L = 0.05 m), **c** optimal design without CMS(L = 0.10 m), **d** optimal design with CMS(L = 0.10 m), **e** optimal design without CMS (L = 0.15 m), **f** optimal design with CMS (L = 0.15 m), **g** evolution histories of the objective function and computation time with different methods

Table 3 Comparison of DOFs for different models

	Component A	Component B	Interface	Full model	Mode synthesis
L = 0.05 m	8526	6762	322	14,966	722
L = 0.10 m	10,136	5152	322	14,966	722
L = 0.15 m	11,746	3542	322	14,966	722

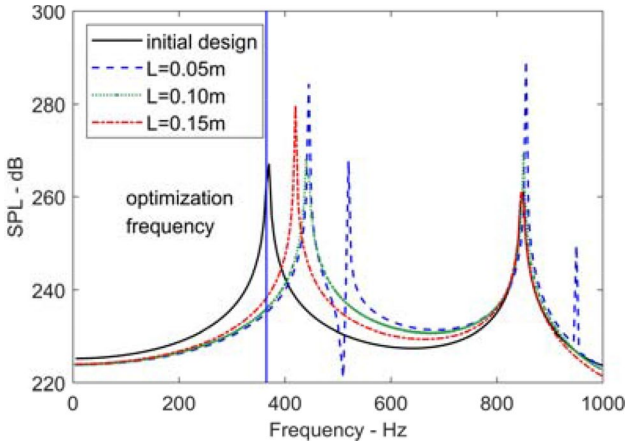

Fig. 9 Comparison of sound pressure level at the reference area under different excitation frequencies. **a** $L=0.05$ m, **b** $L=0.10$ m, **c** $L=0.15$ m

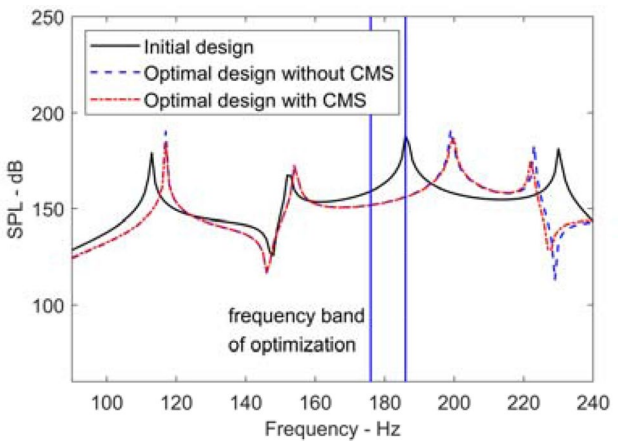

Fig. 11 Comparison of sound pressure level at the reference point under different excitation frequencies for the initial and the optimal design

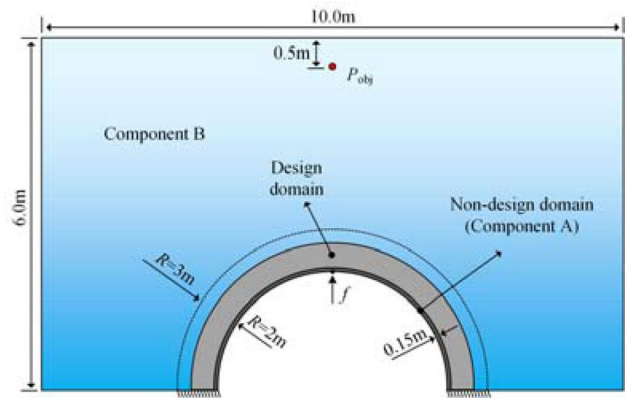

Fig. 10 Geometric properties and boundary conditions of arched beam

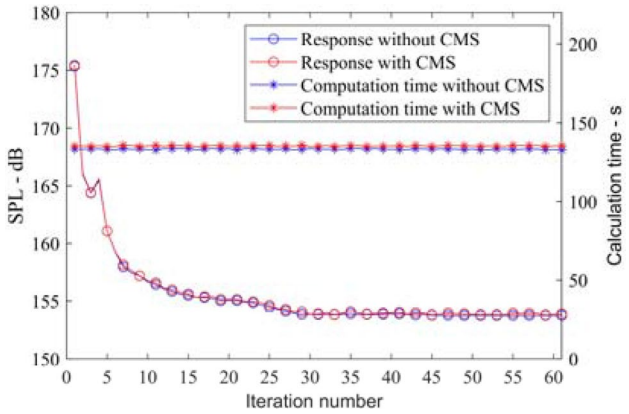

Fig. 12 Evolution histories of the objective function and computation time with different methods

cost without reducing accuracy. The sound pressure level after single-object optimization and multiobject optimization can be effectively reduced. A study of the size of the non-design domain finds that too large a non-design domain is detrimental to the optimization results. The mechanism of reducing the response value at the excitation frequency by optimization iteration is that the resonance frequency of the acoustic vibration coupling system is reduced or increased to avoid the response peak.

In addition, this study was conducted without damp, but damping materials and sound-absorbing materials have effects on sound suppression. Therefore, it is necessary to conduct further research in combination with the mode synthesis method.

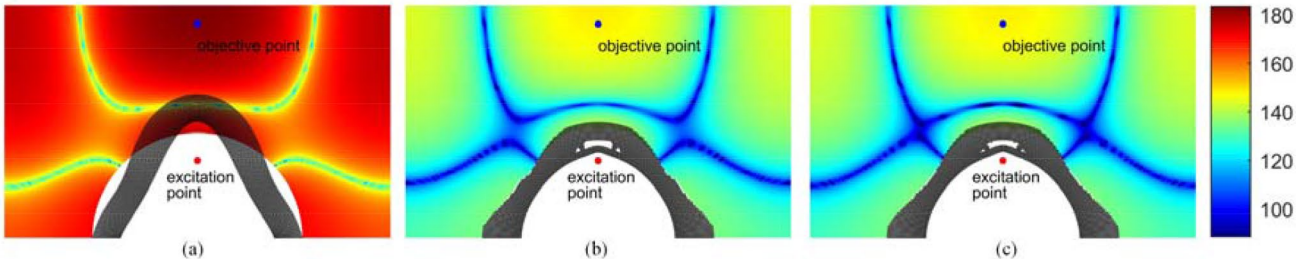

Fig. 13 Contour plots for the initial design and final optimization result at 186 Hz. **a** Initial guess design, **b** optimized design without CMS, **c** optimal design with CMS

Acknowledgements This study is supported by the Chinese National Natural Science Fund (No. 11602300).

Compliance with Ethical Standards

Conflict of interest The authors declare that there is no conflict of interests regarding the publication of this article.

References

1. Akl, W., El, S.A., Al, M.K., et al.: Topology optimization of a plate coupled with acoustic cavity. Int. J. Solids Struct. **46**, 2060–2074 (2009)
2. Vicente, W.M., Picelli, R., Pavanello, R., et al.: Topology optimization of frequency responses of fluid–structure interaction systems. Finite Elem. Anal. Des. **98**, 1–13 (2015)
3. Chen, L.L., Liu, L.C., Zhao, W.C., et al.: 2D Acoustic design sensitivity analysis based on adjoint variable method using different types of boundary elements. Acoust Aust **44**, 343–357 (2016)
4. Xu, Z.S., Huang, Q.B., Zhao, Z.G.: Topology optimization of composite material plate with respect to sound radiation. Eng. Anal. Boundary Elem. **35**, 61–67 (2011)
5. Yoon, G.H., Jensen, J.S., Sigmund, O.: Topology optimization of acoustic structure interaction problems using a mixed finite element formulation. Int. J. Numer. Meth. Eng. **70**, 1049–1075 (2007)
6. Chu, D.N., Xie, Y.M., Hira, A., et al.: Evolutionary structural optimization for problems with stiffness constraints. Finite Elem. Anal. Des. **1996**(21), 239–251 (1996)
7. Jensen, J.S.: Topology optimization of dynamics problems with PADE approximants. Int. J. Numer. Meth. Eng. **72**, 1605–1630 (2010)
8. Allaire, G., Michailidis, G.: Modal basis approaches in shape and topology optimization of frequency response problems. Int. J. Numer. Methods Eng. **113**, 1258–1299 (2018)
9. Kang, Z., Zhang, X., Jiang, S., et al.: On topology optimization of damping layer in shell structures under harmonic excitations. Struct. Multidiscipl. Optim. **46**, 51–67 (2012)
10. Choi, W.S., Park, G.J.: Structural optimization using equivalent static loads at all time intervals. Comput. Methods Appl. Mech. Eng. **191**, 2105–2122 (2002)
11. Zhao, J., Wang, C.: Dynamic response topology optimization in the time domain using model reduction method. Struct. Multidiscipl. Optim. **53**, 101–114 (2016)
12. Lee, H.A., Park, G.J.: Nonlinear dynamic response topology optimization using the equivalent static loads method. Comput. Methods Appl. Mech. Eng. **283**, 956–970 (2015)
13. Teng, X.Y., Jiang, X.D., Sun, Y.X., et al.: Structural topology optimization using equivalent static load and mode tracking. J. Vib. Eng. **3**, 349–356 (2017)
14. Craig, J.R.R., Bampton, M.C.: Coupling of subcomponents for dynamic analyses. AIAA J. **6**, 1313–1319 (1968)
15. Kim, J.G., Lee, P.S.: An enhanced Craig–Bampton method. Int. J. Numer. Methods Eng. **103**, 79–93 (2015)
16. Go, M.S., Lim, J.H., Kim, J.G., Hwang, K.R.: A family of craig–bampton methods considering residual mode compensation. Appl. Math. Comput. **369**, 1–15 (2020)
17. Herrmann, J., Maess, M., Gaul, L.: Substructuring including interface reduction for the efficient vibro-acoustic simulation of fluid-filled piping systems. Mech. Syst. Signal Process. **24**, 153–163 (2010)
18. Maess, M., Gaul, L.: Substructuring and model reduction of pipe components interacting with acoustic fluids. Mech. Syst. Signal Process. **20**, 45–64 (2006)
19. Kim, S.M., Kim, J.G., Chae, S.W., et al.: A strongly coupled model reduction of vibro-acoustic interaction. Comput. Methods Appl. Mech. Eng. **347**, 495–516 (2019)
20. Morand, H.J.P., Roger, O.: Fluid Structure Interaction-Applied Numerical Methods. Wiley, Paris (1995)
21. Sandberg, G., Wernberg, P.A., Davidsson, P.: Fundamentals of Fluid–Structure Interaction, vol. 505. Springer, Vienna (2008)
22. Du, J.B., Wang, X.C.: Fluid–structure coupling dynamic characteristic analysis for rotationally periodic liquidfilled vessel (I). J. Tsinghua **39**, 108–111 (1999)
23. Du, J.B., Wang, X.C.: Fluid–structure coupling dynamic characteristic analysis for rotationally periodic liquid-filled vessel (II). J. Tsinghua **39**, 112–116 (1999)
24. Huang, X., Xie, Y.M.: Convergent and mesh independent solutions for the bi-directional evolutionary structural optimization method. Finite Elem. Anal. Des. **43**, 1039–1049 (2007)